Acta Oceanol. Sin., 2019, Vol. 38, No. 4, P. 154–166
https://doi.org/10.1007/s13131-019-1419-1
http://www.hyxb.org.cn
E-mail: hyxbe@263.net

Development of a fine-resolution atmosphere-wave-ocean coupled forecasting model for the South China Sea and its adjacent seas

Junchuan Sun[1, 2], Zexun Wei[1, 2], Tengfei Xu[1, 2], Meng Sun[1, 2], Kun Liu[1, 2], Yongzeng Yang[1, 2], Li Chen[3], Hong Zhao[3], Xunqiang Yin[1, 2], Weizhong Feng[4], Zhiyuan Zhang[5], Yonggang Wang[1, 2*]

[1] Key Laboratory of Marine Science and Numerical Modeling, First Institute of Oceanography, Ministry of Natural Resources, Qingdao 266061, China

[2] Laboratory for Regional Oceanography and Numerical Modeling, Qingdao National Laboratory for Marine Science and Technology, Qingdao 266237, China

[3] National Marine Environmental Forecasting Center, Ministry of Natural Resources, Beijing 100081, China

[4] South China Sea Marine Prediction Center, Ministry of Natural Resources, Guangzhou 510310, China

[5] Hydro-Meteorological Center of Navy, PLA, Beijing 100161, China

Received 23 March 2018; accepted 29 June 2018

Abstract

A 72-h fine-resolution atmosphere-wave-ocean coupled forecasting system was developed for the South China Sea and its adjacent seas. The forecasting model domain covers from from 15°S to 45°N in latitude and 99°E to 135°E in longitude including the Bohai Sea, the Yellow Sea, the East China Sea, the South China Sea and the Indonesian seas. To get precise initial conditions for the coupled forecasting model, the forecasting system conducts a 24-h hindcast simulation with data assimilation before forecasting. The Ensemble Adjustment Kalman Filter (EAKF) data assimilation method was adopted for the wave model MASNUM with assimilating Jason-2 significant wave height (SWH) data. The EAKF data assimilation method was also introduced to the ROMS model with assimilating sea surface temperature (SST), mean absolute dynamic topography (MADT) and Argo profiles data. To improve simulation of the structure of temperature and salinity, the vertical mixing scheme of the ocean model was improved by considering the surface wave induced vertical mixing and internal wave induced vertical mixing. The wave and current models were integrated from January 2014 to October 2015 driven by the ECMWF reanalysis 6 hourly mean dataset with data assimilation. Then the coupled atmosphere-wave-ocean forecasting system was carried out 14 months operational running since November 2015. The forecasting outputs include atmospheric forecast products, wave forecast products and ocean forecast products. A series of observation data are used to evaluate the coupled forecasting results, including the wind, SHW, ocean temperature and velocity. The forecasting results are in good agreement with observation data. The prediction practice for more than one year indicates that the coupled forecasting system performs stably and predict relatively accurate, which can support the shipping safety, the fisheries and the oil exploitation.

Key words: South China Sea, COAWST model, MASNUM model, atmosphere-wave-ocean forecasting system, data assimilation

Citation: Sun Junchuan, Wei Zexun, Xu Tengfei, Sun Meng, Liu Kun, Yang Yongzeng, Chen Li, Zhao Hong, Yin Xunqiang, Feng Weizhong, Zhang Zhiyuan, Wang Yonggang. 2019. Development of a fine-resolution atmosphere-wave-ocean coupled forecasting model for the South China Sea and its adjacent seas. Acta Oceanologica Sinica, 38(4): 154–166, doi: 10.1007/s13131-019-1419-1

1 Introduction

The South China Sea, with an area of about 3.5 million km^2, is the largest semi-enclosed marginal sea in the Northwest Pacific, and it connects with the Pacific through the Luzon Strait and with the East China Sea through the Taiwan Strait. In the south, it exchanges water with the Sulu Sea through the Mindoro Strait and with the Java Sea through the Karimata Strait. The South China Sea is the key region for the 21st Century Maritime Silk Road, leading to increasingly attention for marine environment related prediction, such as marine disaster, navigation, oil spilling, maritime search and rescue. Of these issues, it requires accurate forecast of marine meteorological elements including sea surface wind, sea level, marine temperature, ocean waves and currents.

The advantage of the wind-wave-current coupled model has been recognized since the 1960s, Manabe and Bryan (1969) conducted an ocean-atmosphere coupled numerical simulation with ideal geometry. This coupled scheme was updated to consider real topography (Manabe et al., 1975; Bryan et al., 1975; Washington et al., 2010). Recently, benefit to the rapidly development of high performance computing, the coupled models are design

Foundation item: The National Key Research and Development Program of China under contract No. 2017YFC1404201; the NSFC-Shandong Joint Fund for Marine Science Research Centers under contract No. U1606405; the SOA Program on Global Change and Air-Sea Interactions under contract Nos GASI-IPOVAI-03 and GASI-IPOVAI-02; the National Natural Science Foundation of China under contract Nos 41606040, 41876029, 41776016, 41706035 and 41606036.
*Corresponding author, E-mail: ygwang@fio.org.cn

with high resolution, full coupled with complex physical process, and regional focus (Boville and Gent, 1998; Collins et al., 2006; Seo et al., 2007; Neelin et al., 1992). The US navy developed a two-way regional atmosphere-ocean coupled model COAMPS in 1997, which has been update to COAMPS3.1.1 in 2004 (Hodur, 1997). Gustafsson et al. (1998) set up a regional atmosphere-ocean coupled model with considering sea-ice for the weather prediction in the Baltic Sea. Hagedorn et al. (2000) coupled the atmosphere model REMO with the ocean model BSMO to predict the SST in the Baltic Sea, indicating that the air-sea coupling is capable of improving the skill of SST prediction. Döscher et al. (2002) developed a regional ocean-atmosphere-sea-ice coupled model RCAO. Schrum et al. (2003) coupled the atmosphere model REMO and the ocean model HAMSOM with full coupling process. Aldrian et al. (2005) developed a regional coupled model based on REMO and MPI-OM to study the air-sea interaction over the Indonesian seas. Sasaki et al. (2006) coupled a high-resolution atmosphere model RCM20 to an ocean model that covers the North Pacific using nested method to simulate climate variability in Japan. Seo et al. (2007) coupled the ROMS ocean model to RSM atmosphere model to investigate the air-sea interaction over the East Pacific. Bruneau and Toumi (2016) developed a fully-coupled atmosphere-ocean-wave model of the Caspian Sea and conducted a series of experiments to study the ocean wave of the Caspian Sea.

In this study, we develop a fully-coupled atmosphere-wave-ocean model which covers the South China Sea and its adjacent seas to forecast the sea surface wind, sea level, marine temperature, ocean waves and currents. The forecast system is designed to have 72 h forecast ability, with pre-24-h hindcast with data assimilation for precise initial conditions of the wave and ocean models. The paper is organized as follows: after introduction, some details on coupled model description are provided; and then the comparison of coupled forecasting results with independent observations is shown. The last part is conclusions.

2 Model description

The Coupled-Ocean-Atmosphere-Wave-Sediment Transport (COAWST) Modeling System was developed by Warner et al. (2008, 2010), which is comprised of four components including the ocean model, the wave model, the atmosphere model and the sediment transport model. The MCT was adopted as the coupler to exchange data fields between the different components. In this paper, on the base of the COAWST modeling system and the MASNUM wave model, a 72-h fine-resolution coupled atmosphere-wave-ocean forecasting system was developed for the South China Sea and its adjacent seas. This section gives a brief introduction to the coupled forecasting system.

2.1 *Atmosphere model*

The atmospheric model component employed in the COAWST model system is the Advanced Weather Research and Forecasting model (WRF 3.6.1, Skamarock et al., 2005). It is a non-hydrostatic, quasi-compressible atmospheric model which has been widely used for idealized and realistic research of numerical experiments as well as for the forecast systems. The WRF model uses the Arakawa-C grid and the sigma-pressure vertical coordinate grid. In the coupled forecasting system, the WRF model covers the South China Sea and its adjacent seas (15°S–45°N, 99°–135°E, Fig. 1), with a horizontal resolution of (1/36)°×(1/36)° and 31 sigma levels in the vertical. The lateral open boundaries and initial conditions are derived from the National Centers for Environmental Prediction (NCEP) Global Forecast Model (GFS) (http://www.nco.ncep.noaa.gov/pmb/products/gfs/) with 1°×1° resolution and 6-h interval.

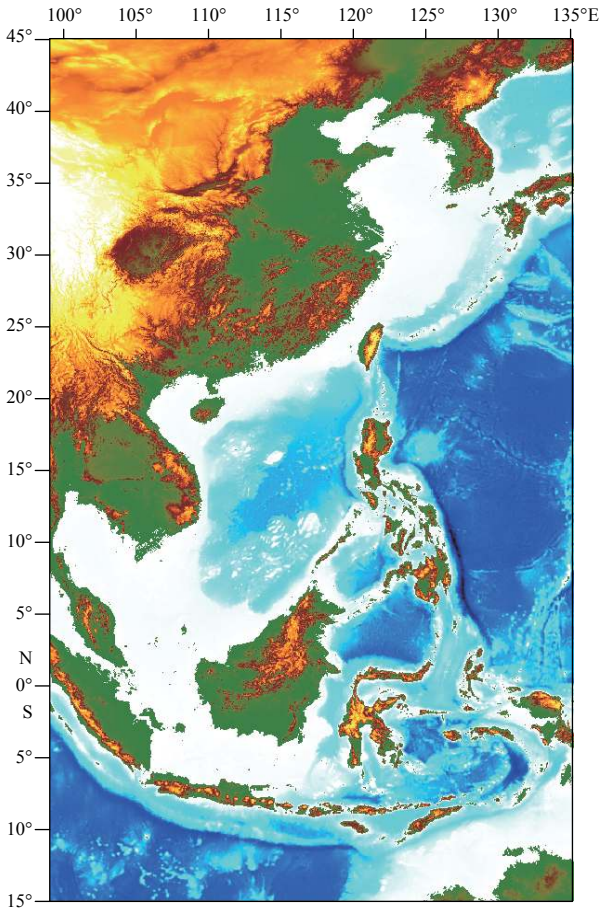

Fig. 1. Domains of the atmosphere-wave-ocean coupled forecasting model.

The WRF model has a variety of physical parameterizations for sub-grid-scale processes including microphysics, long-wave and short-wave radiation, planet boundary layer, land surface, surface layer and cumulus, etc. The physical parameterizations used in the coupled forecasting system are listed in Table 1.

Table 1. Physical parameterizations used for the WRF model

Parameterization	Physics options	Reference
Microphysics	Single-Moment 6-class scheme	Hong et al. (2006)
Long–wave radiation	RRTM scheme	Mlawer et al. (1997)
Short–wave radiation	Dudhia scheme	Dudhia (2004)
Cumulus	Kain–Fritsch scheme	Kain (2004)
Surface layer	Eta similarity	Janjic (1996, 2002)
Land surface	Noah land surface scheme	Chen and Dudhia (2001)
Planet boundary layer	Yonsei University PBL scheme	Hong and Pan (1998)

2.2 *The SWAN wave model*

The wave model component adopted in the COAWST model system is SWAN 40.91A (Simulating WAves Nearshore), which is a third-generation spectral wave model specifically designed for shallow water simulation (Booij et al., 1999). SWAN solves the spectral density evolution equation and can simulate wind wave generation and propagation in coastal waters including the processes of refraction, diffraction, shoaling, wave–wave interactions, etc. (Warner et al., 2010). In the coupled forecasting system, SWAN uses the same grid as WRF and the bathymetry is extracted from the ETOPO1 data set, supplied by National Geophysical Data Center (NGDC). The lowest and highest discrete frequency is set to 0.042 and 0.42, respectively. The spectral directional resolution is 15°. The JONSWAP spectrum (Hasselmann et al., 1973) is used for the boundary condition and the initial condition is derived from the MASNUM wave model with assimilating Jason-2 SHW data.

2.3 *The MASNUM wave model*

The MASNUM wave model was first presented by Yuan et al. (1991, 1992), developed to global scale by Yang et al. (2005) and parallelized by Wang et al. (2010a). The complicated characteristic inlaid method is applied to integrate the wave energy spectrum balance equation. In the MASNUM, the wave energy spectrum balance equation and its complicated characteristic equations are derived in a wave-number space. The breaking dissipation source function adopted a theoretical result based on a statistical study of breaking waves (Yuan et al., 1986). In the coupled forecasting system, MASNUM uses the same grid and bathymetry as SWAN. The model simulates the 2-D spectrum of wave energy discretized into 24 directional bands, 15° wide, and 25 frequency bands spaced from 0.042 to 0.42 Hz. The propagation time step is 5 min.

Anderson (2001, 2003) proposed Ensemble Adjustment Kalman filter (EAKF), where the analysis is computed without adding perturbations to the observations. In this method, a linear operator which replaces the traditional gain matrix was introduced. This method makes it possible to obtain reliable results for small ensembles (10–20 members) (Evensen, 2003). However, high computational cost due to model ensemble in EAKF is employed. In this study, the 24-h interval difference of simulated SWH is used to construct static ensemble (Sun et al., 2014, 2017), which approximates the background error. The static ensemble is superposed to the simulated SWH field at assimilation time to obtain ensemble states and then update ensemble states using EAKF. Thus, only one wave model sample is required to run and the computational cost is reduced sharply.s

2.4 *Ocean model*

The ROMS model is a three-dimensional, hydrostatic, free surface, terrain-following coordinate (s-coordinate) numerical ocean model which solves the Reynolds-Averaged Navier–Stokes equations using the Boussinesq and hydrostatic assumptions (Haidvogel et al., 2002; Chassignet et al., 2003) with a split-explicit time stepping algorithm (Shchepetkin and McWilliams, 2005; Haidvogel et al., 2008; Shchepetkin and McWilliams, 2009). The ROMS model (svn 748) was adopted in the COAWST modeling system. For the coupled forecasting system, the ROMS model also use the same grid and bathymetry as SWAN and MASNUM, with a horizontal resolution of (1/36)°×(1/36)° and 30 s-coordinate levels in the vertical. To get precise initial conditions for the ocean model in the coupled forecasting system, an uncoupled ROMS model is set up synchronously. The procedure includes three steps.

First, for spin-up of the ocean model, the climatological simulation is integrated for 40 years from the initial conditions. The climatology monthly mean temperature and salinity in January derived from Generalized Digital Environmental Model (GDEM) Version 3.0 dataset (Carnes, 2009) are used to initialize the model. The surface forcing is derived from the Comprehensive Ocean-Atmosphere Data Set (COADS), which are composed of the climatological monthly mean SST, wind stresses, net heat flux, surface solar shortwave radiation, net fresh water flux, and sea surface salinity (Diaz et al., 2002). In addition, the surface net heat flux sensitivity to SST (dQ/dSST) derived from bulk formulas is used to introduce net heat flux correction as a function of model SST minus forcing SST. The lateral open boundaries are obtained from spatial interpolation of the climatological simulation from Ocean General Circulation Models for the Earth Simulator (OFES). The sponge layers with larger viscosity coefficients are used for the damping of high frequency noise due to open boundary conditions. The monthly mean discharges of 16 major rivers (Huanghe River (Yellow River), Changjiang River, Zhujiang River (Pearl River), Mekong River, etc.) are added to the model. On the other hand, the KPP mixing scheme is adopted in the ocean model with common setting. The nonbreaking wave-induced mixing (B_v; following the abbreviated form of Qiao et al. (2004)) is introduced by simply adding to the KPP derived vertical viscosity and diffusivity (Wang et al., 2010b). B_v is expressed by Qiao et al. (2004, 2010) as the following equation:

$$B_v = \alpha \int\int E\left(\vec{k}\right) \exp\{2kz\}\, \mathrm{d}\vec{k} \times \frac{\partial}{\partial z}\left(\int\int_k \omega^2 E\left(\vec{k}\right) \exp\{2kz\}\, \mathrm{d}\vec{k}\right)^{\frac{1}{2}}, \quad (1)$$

where α is constant and set to 0.2, ω is wave angular frequency, k is wave number, z is depth (downward positive with z=0 at the surface), and $E\left(\vec{k}\right)$ represents the wave number spectrum. The B_v is computed directly by the MASNUM wave model driven by the climatological monthly mean wind stresses from COADS. Meanwhile, the South China Sea is considered a hotpot of turbulent mixing due to the high-frequency nonlinear internal waves (Laurent, 2008). On the base of parameterization and hydrographic observations, a three-dimensional distribution of turbulent mixing in the SCS is obtained by Yang et al. (2016). Similar to the B_v, the internal wave induced vertical mixing is interpolated into the ROMS grid and included by simply adding to the KPP derived vertical viscosity and diffusivity.

Second, the hindcast simulation initialized from the end month of climatology run and were integrated from January 2014 to October 2015 driven by the 6 hourly mean wind stresses, net heat fluxes, net fresh water fluxes, and surface solar shortwave radiation derived from the ERA—interim dataset. The lateral open boundaries are obtained from spatial interpolation of the global ocean forecasting system developed by the First Institute of Oceanography (FIO), Ministry of Natural Resources. The EAKF data assimilation method was adopted for the hindcast simulation (Yin et al., 2010). A random field scheme (Evensen, 1994) was used to construct the wind forcing field ensemble, which can be written as the following equation:

$$W^{\mathrm{a}}_{i,j,n} = W^{\mathrm{b}}_{i,j} + \alpha_{B_n} \cdot \lambda_{i,j,n}, \quad (2)$$

where $W^{\mathrm{b}}_{i,j}$ and $W^{\mathrm{a}}_{i,j,n}$ are the wind forcing field before and after the perturbation, respectively; $\lambda_{i,j,n}$ are the random field; α_{B_n} is

the ratio of standard deviation between the wind field and the random, which is used to control the amplitude of the perturbation; subscripts n =1, 2, ..., N is the ensemble index where N is ensemble size. In this study, 10 wind forcing field ensembles are constructed. The assimilation system developed by Yin et al. (2010) based on the EAKF method was incorporated with the ROMS model. The daily Argo temperature and salinity profiles data, the Microwave and Infrared Optimally Interpolated Sea Surface Temperature daily products (MI_IR SST) and the daily Mean Absolute Dynamic Topography (MADT) are assimilated into the hindcast simulation. After being integrated from January 2014 to October 2015, the pre-24-h assimilated ocean hindcast simulation was run to provide the initial condition for the coupled forecasting system.

2.5 *Coupled forecasting system*

Figure 2 illustrates the procedure of the coupled forecasting system, which is arranged by using UNIX shell scripts. The coupled forecasting system is mainly composed of three parts. In the first part, the system will carry out a series of preprocess, in turn, downloading the GFS data and preparing the lateral open boundaries and initial conditions for the WRF model, downloading the global ocean forecast data and preparing the lateral open boundaries for the ROMS model, downloading and preprocessing the observation data for assimilation, extracting the forcing data for the 24-h hindcast simulation with data assimilation including the ROMS model and MASNUM wave model from the latest WRF forecasting results. In the second part, the stand-alone MASNUM will run with data assimilation, outputting the wave induced mixing parameter B_v for the stand-alone ROMS model and providing the initial field for the SWAN model in the coupled forecasting system. After that, the stand-alone ROMS model will run with data assimilation, outputting the initial field for the ROMS model in the coupled forecasting system. Then, the 72-h coupled forecasting model runs eventually. The last part is postprocessing, including the forecast verification and the visualization. After the postprocess finished, the forecast data will be backed up automatically.

The operational monitoring system is developed based on the UNIX operating system, the Common Gateway Inteface (CGI) and the Telnet protocol to realize remote monitoring and manage the forecast system. The monitoring system can supervisory control each step of the forecast system and provide abnormal alert.

3 Forecast verification

Several kinds of observation data (Table 2) are used to assess and improve the coupled forecasting system, including the ocean station data, the optimum interpolation sea surface temperature (OISST), the Argo temperature profile, the continuous current data and the Buoy observation data. Figure 3a shows the observing stations of the Argo profile from November 2016 to December 2016. Figure 3b shows the *in-situ* stations. The red dots denote the ocean station, the red star denotes the seabed

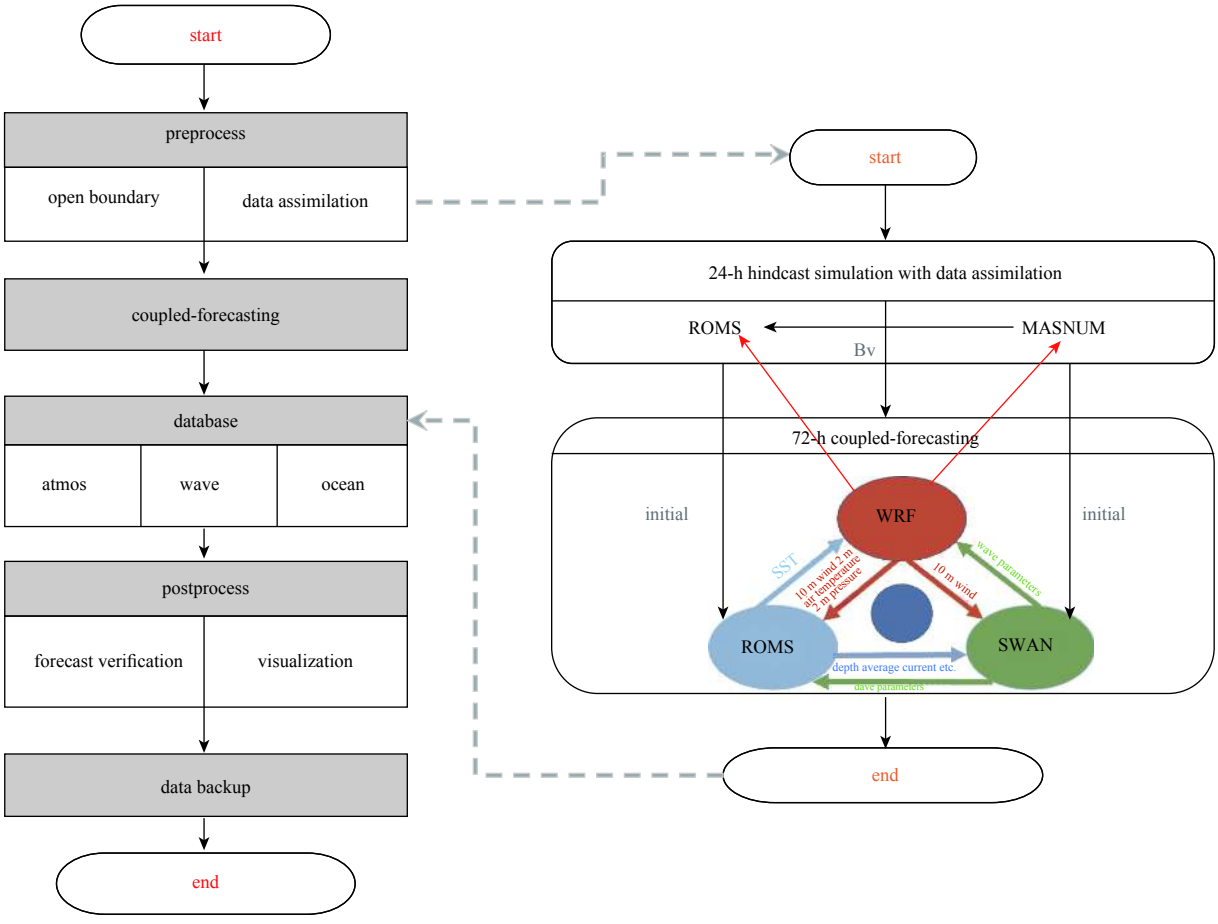

Fig. 2. A schematic illustration of the coupling between the WRF, ROMS and SWAN and the procedure of the coupled forecasting system. The MASUNM wave model provides nonbreaking wave-induced vertical mixing to the ROMS model and provides initial conditions to the SWAN model.

platform, the blue asterisks denote the buoy, and the black asterisks denote the sites selected for the SST comparison, respectively.

Figures 4 and 5 show the comparisons of wind speed and dir-

Table 2. Summary of observation data used for forecast verification

Elements	Data names	Data source	Comments
Wind	ocean station data	National Marine Environmental Forecasting Center	surface wind (10 m)
Temperture	OISST	ftp.discover-earth.org	sea surface temperature
	Argo	ftp://ftp.ifremer.fr/ifremer/Argo	temperature profile
Current	continuous current data	seabed platform in Karimata Strait	ADCP
Wave	buoy observation data	State Oceanic Administration ocean observation net and Taiwan Central Weather Bureau	significant wave height

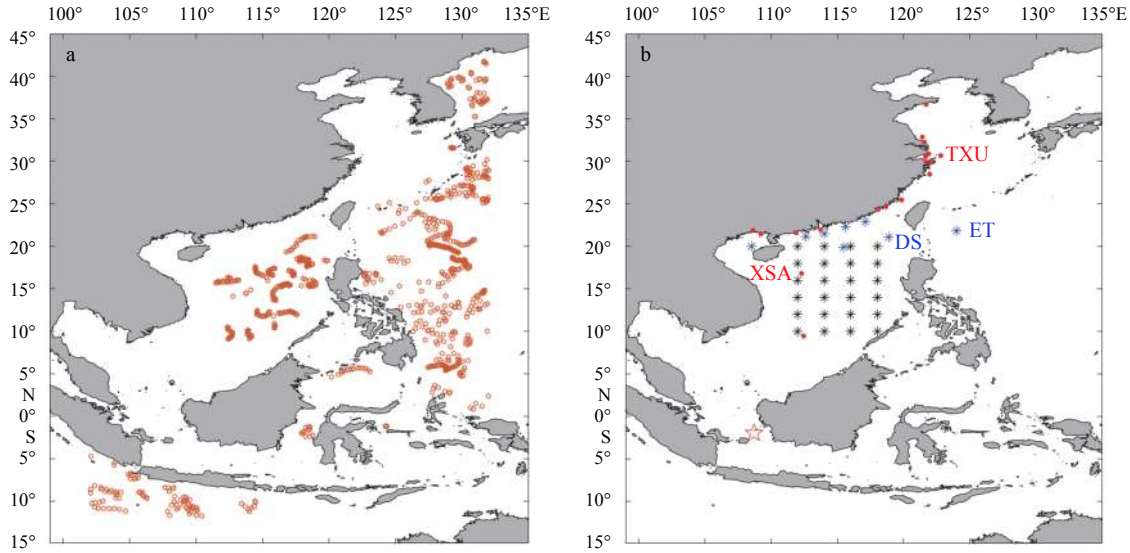

Fig. 3. Observing stations of the Argo profile (a) and the *in-situ* stations (b). The red dots denote the ocean station, the red stars the seabed platform, the blue asterisks the buoy, and the black asterisks the sites selected for the sea surface temperature comparison.

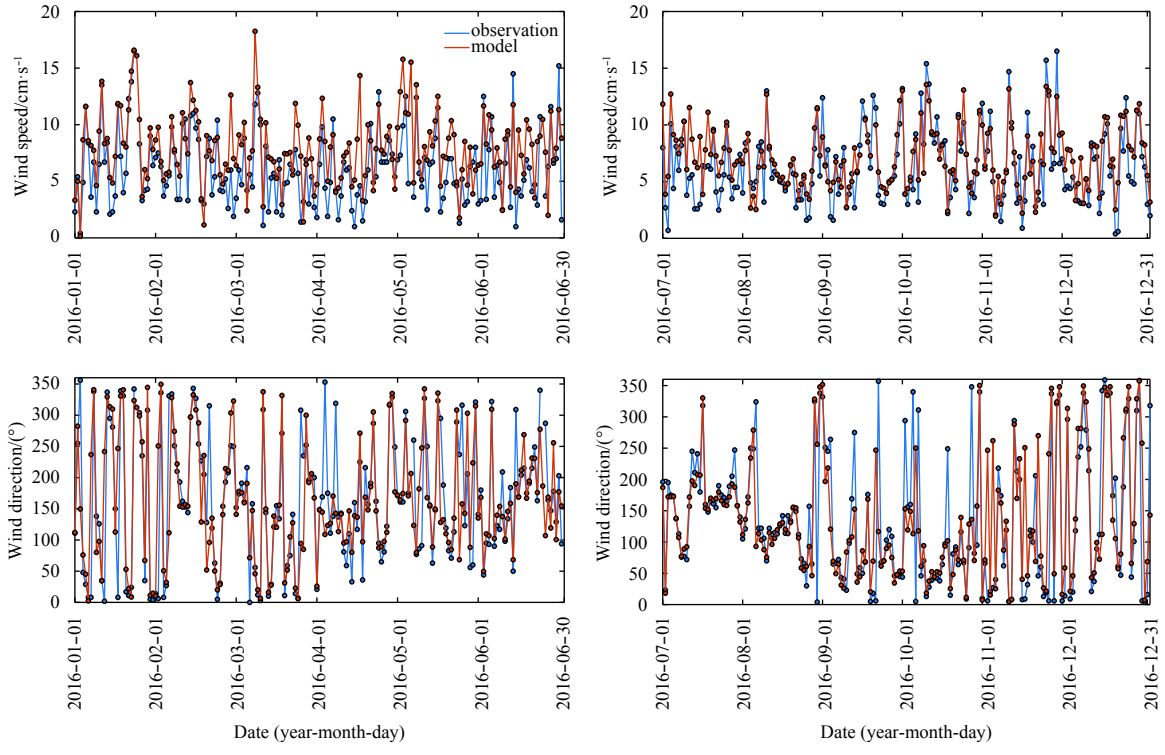

Fig. 4. Comparison of wind speed and direction at TXU between observation (red line) and 72-h forecasting results (blue line).

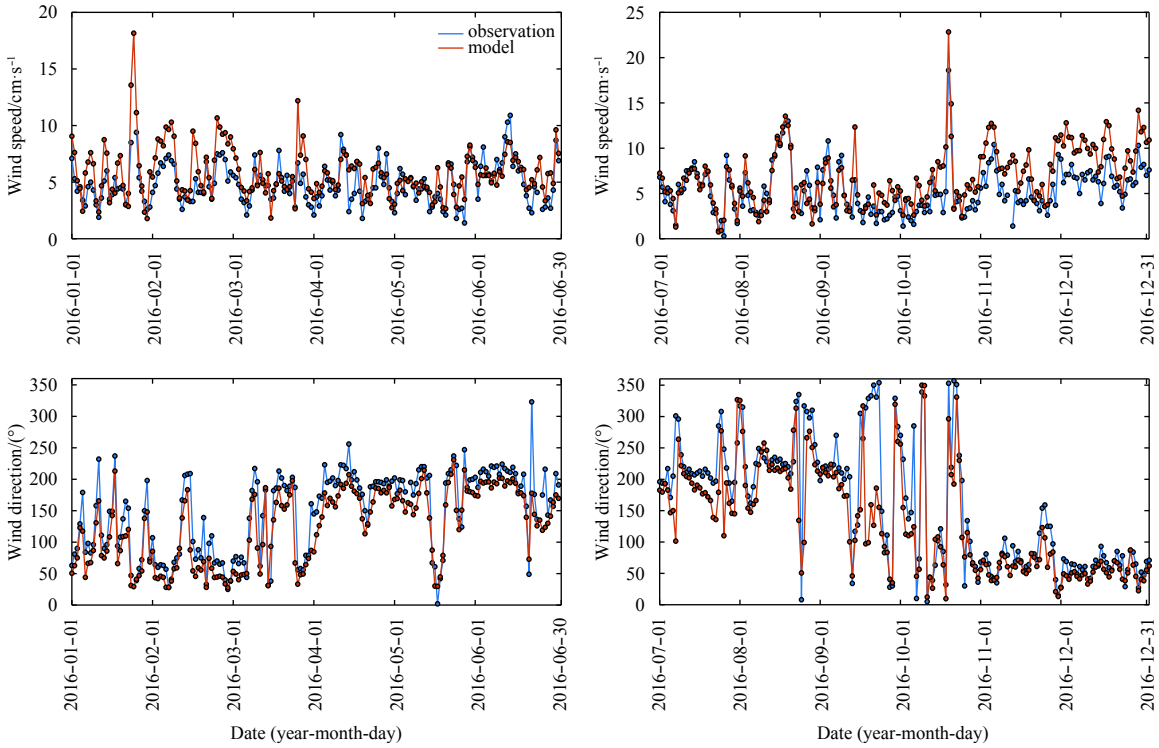

Fig. 5. Comparison of wind speed and direction at XSA between observation (red line) and 72-h forecasting results (blue line).

ection between the observation of two ocean stations (the TXU and XSA in Fig. 3) and 72-h forecasting results from January 2016 to December 2016. The 72-h forecasting wind components agree well with the observation during the year except for the monsoon change, the forecasting error range is relatively large during the monsoon transition period. As shown in Fig. 4, the difference of wind direction between the observation and 72-h forecasting results is much bigger in April and October. The statistical analyses of the coherence for wind speed and direction between the observation of 18 ocean stations and 72-h forecasting results are listed in Table 3. The mean absolute errors (MAE) of wind speed (wind direction) for 18 ocean stations range from 1.68 m/s (10.19°) to 2.17 m/s (29.32°). The relative errors (RE) of wind speed (wind direction) for 18 ocean stations range from 8.35% (28.27%) to 29.29% (40.36%). The root-mean-square errors (RMSE) of wind speed (wind direction) for 18 ocean stations range from 2.12 m/s (12.89°) to 2.75 m/s (37.10°).

Figures 6 and 7 show the comparisons of SWH between the

Table 3. Statistical analysis of the coherence for wind speed and direction between observation and 72-h forecasting results

Oceanic station	Wind speed			Wind direction		
	MAE/m·s^{-1}	RE/%	RMSE/m·s^{-1}	MAE/(°)	RE/%	RMSE/(°)
BHI	2.16	8.90	2.73	14.39	28.27	18.21
BLG	1.88	20.63	2.38	22.65	35.47	28.66
DCN	2.08	12.25	2.63	20.55	33.79	26.00
DWS	1.90	20.00	2.40	28.57	39.84	36.15
JNJ	2.07	12.82	2.62	10.19	23.79	12.89
LCG	1.85	21.90	2.34	21.51	34.57	27.22
LNH	1.94	18.15	2.46	13.76	27.65	17.41
NHD	2.03	14.56	2.56	28.96	40.11	36.64
NSA	1.94	18.15	2.46	27.93	39.39	35.34
PHX	2.12	10.56	2.68	19.88	33.23	25.15
PTN	1.98	16.33	2.51	18.09	31.70	22.89
PZG	2.17	8.35	2.75	19.57	32.97	24.76
QZH	1.79	24.50	2.26	29.32	40.36	37.10
SSN	2.01	15.15	2.55	16.81	30.56	21.27
TXU	1.97	16.93	2.49	17.34	31.04	21.94
ZHI	1.85	21.90	2.34	21.42	34.50	27.10
ZPO	1.68	29.29	2.12	19.68	33.07	24.90
XSA	1.73	27.20	2.18	24.86	37.16	31.46
Average	1.95	17.64	2.47	20.86	34.75	26.39

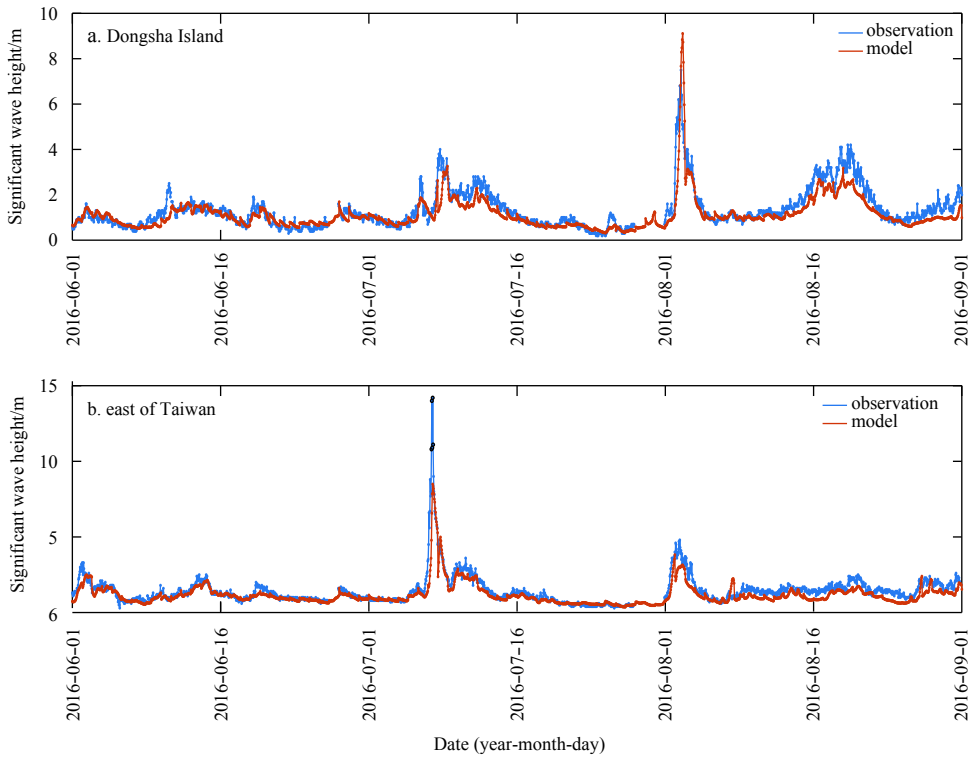

Fig. 6. Comparison of significant wave height between observation (blue line) and 72-h forecasting results (red line). The buoy observation stations are located around the Dongsha Island and east of Taiwan Island.

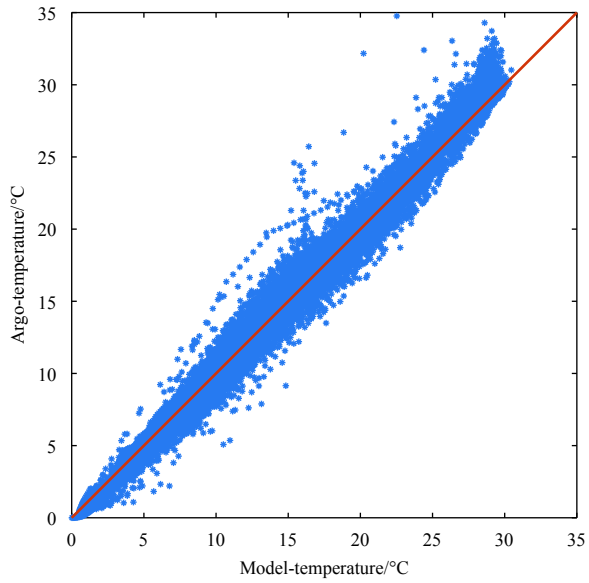

Fig. 7. Temperature scatter points comparing between Argo and 72-h forecasting results.

observations of two buoys (the DS and ET stations in Fig. 3) and 72-h forecasting results from June 2016 to September 2016. Modeled SWH matches well with the *in-situ* data except for the strong wave process. For example, the SWH of Dongsha station is high in August and the difference of SWH in August between the observation and 72-h forecasting results is bigger than June and July (Fig. 6a). Moreover, the maximum forecasting SWH in 8 July 2016 of east of Taiwan station is about 8.3 m (Fig. 6b), which is much smaller than the *in-situ* observation (14.1 m). This means particular efforts should be made to strengthen the prediction ability for the extreme weather process. The statistical analyses of the coherence for SWH between the observation and 72-h forecasting results are listed in Table 4. The average MAE is 0.44 m, the average RE is 23.3% and the average RMSE is 0.55 m.

Figure 7 shows the fitting curve of temperature between Argo profiles and 72-h forecasting results from November 2016 to December 2016. It shows that fitting coefficients of temperature approximate to 1, which indicates a good agreement between the modeled results and the measurements. In addition, the comparison of temperature profiles between some Argo profiles and 72-h forecasting results also indicates a good agreement (Fig. 8). To validate the forecasting SST, the MAE, the RE and the RMSE between modeled SST and OISST data are calculated for each month (Figs 9–11). The simulation of SST is nearly in consistence with the satellite observation in spatial and temporal. The SST er-

Table 4. Statistical analysis of the coherence for significant wave height between observation and 72-h forecasting results

Buoy station	Significant wave height		
	MAE/m	RE/%	RMSE/m
East of Taiwan (ET)	0.50	21.5	0.63
Dongsha (DS)	0.46	22.0	0.58
QF307	0.46	22.5	0.58
QF303	0.44	23.0	0.56
QF305	0.42	23.7	0.53
QF306	0.43	26.7	0.54
QF304	0.38	24.2	0.48
SF304	0.40	22.4	0.51
Average	0.44	23.3	0.55

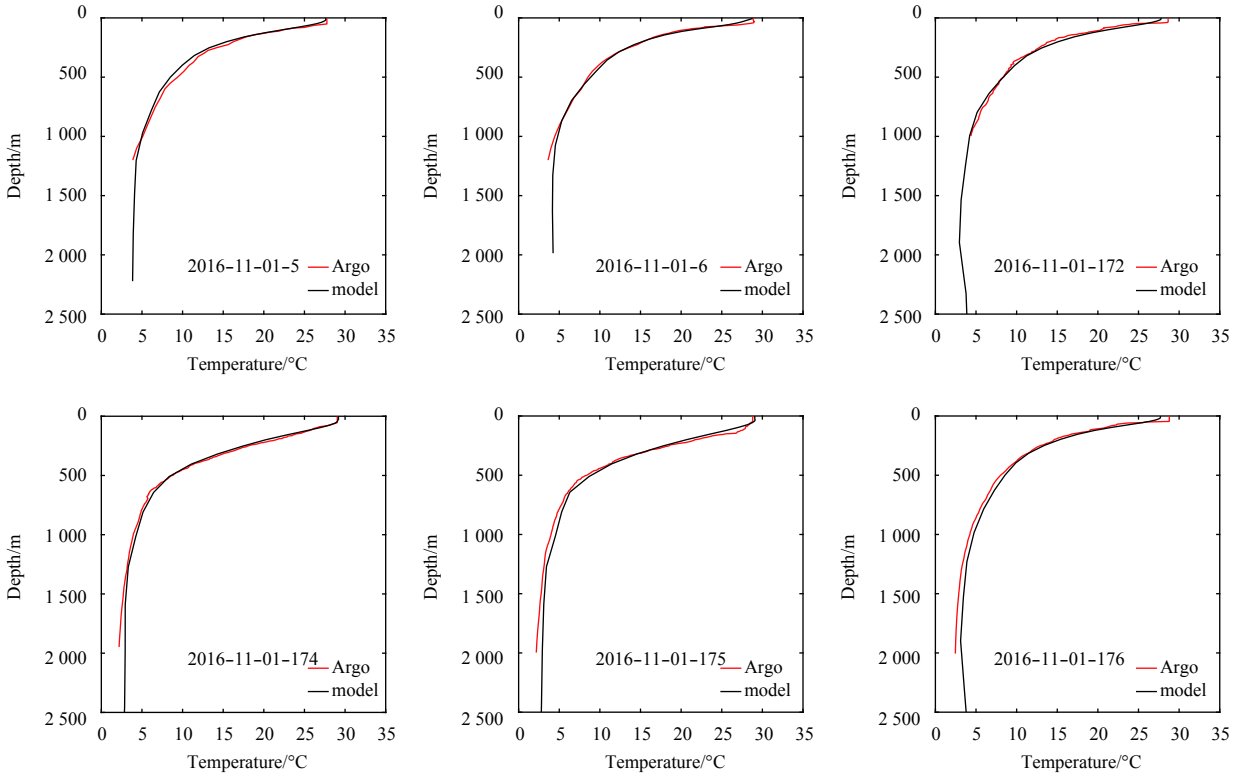

Fig. 8. Comparison of temperature profiles between Argo (red line) and 72-h forecasting results (black line). The number after the date is the number of the valid Argo data in the forecasting model domain.

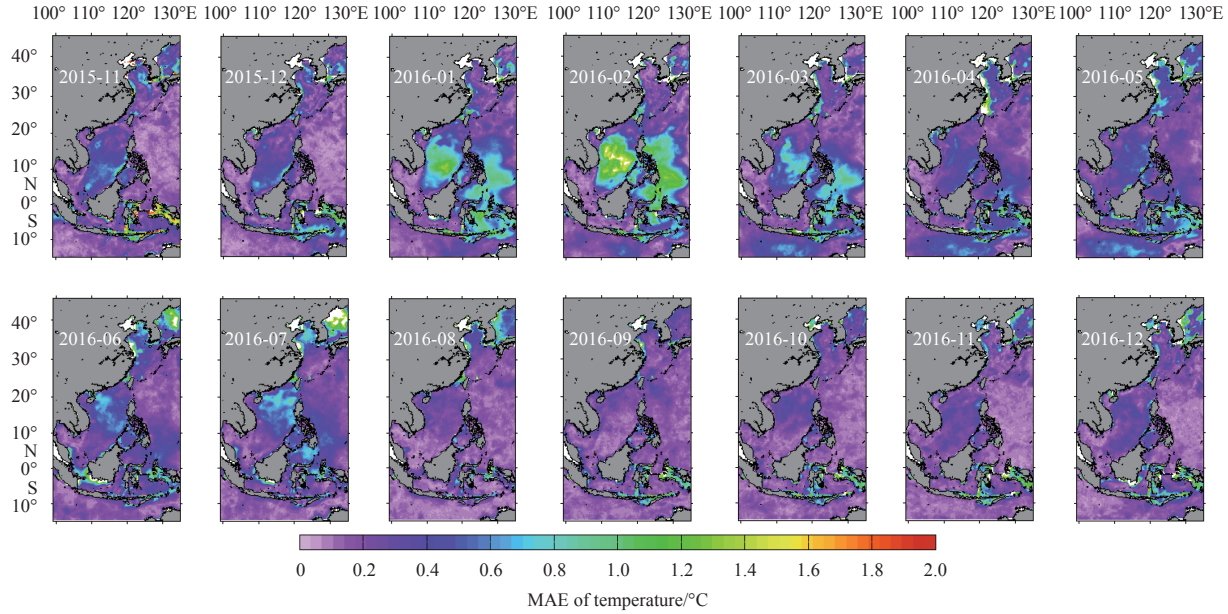

Fig. 9. Spatial distribution of MAE between the monthly mean OISST and the monthly mean 72-h forecasting results.

rors mainly focus on the coastal area, such as the Bohai Sea, the Yellow Sea coastal area and the Indonesia coastal area. This mainly because the satellite remote sensing SST have bias in the coastal area. On the other hand, the difference of SST between the observation and 72-h forecasting results is relative big in the center area of the South China Sea and east of the Philippine islands, possibly because the heat flux bias. Table 5 displays the statistical analysis of the coherence for temperature between the observation (Argo and OISST) and 72-h forecasting results.

Figure 12 shows the comparison of velocity speed and direction between the ADCP data observed in Karimata Strait and 72-h forecasting results. The forecasting currents agree well with the *in-situ* observations, especially the velocity direction. Interestingly, the forecasting results are more consistent with the observations in the deep layer. As shown in Table 6, the MAE of velocity speed (velocity direction) for the upper layer (2 m) is 0.13 m/s

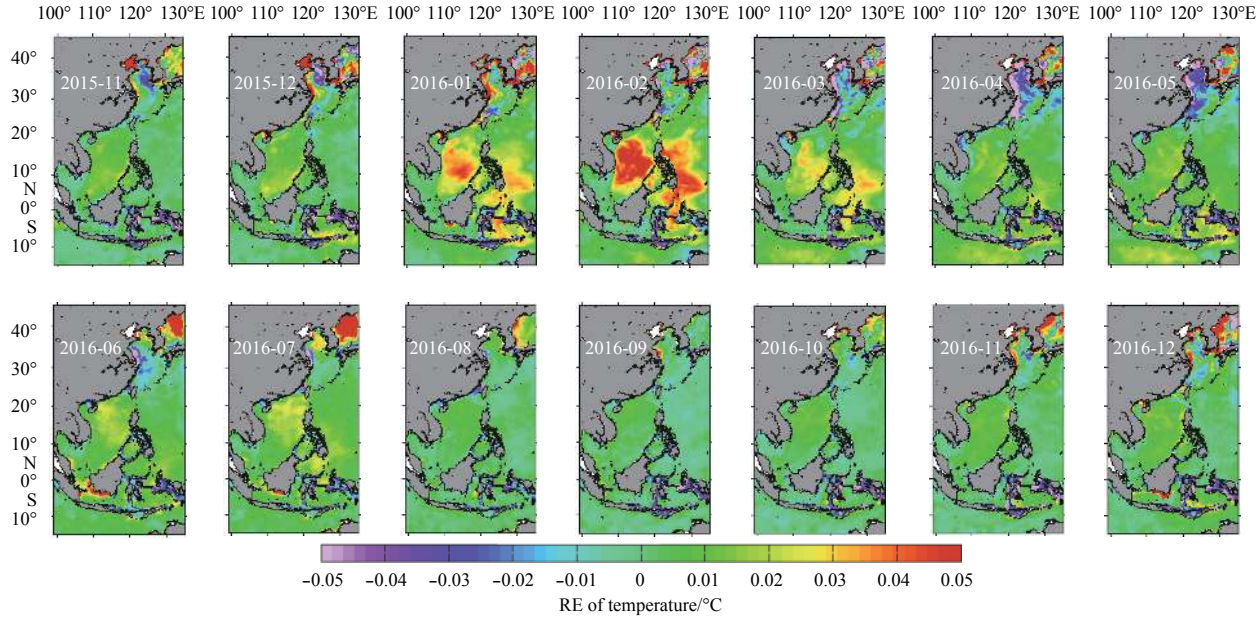

Fig. 10. Spatial distribution of RE between the monthly mean OISST and the monthly mean 72-h forecasting results.

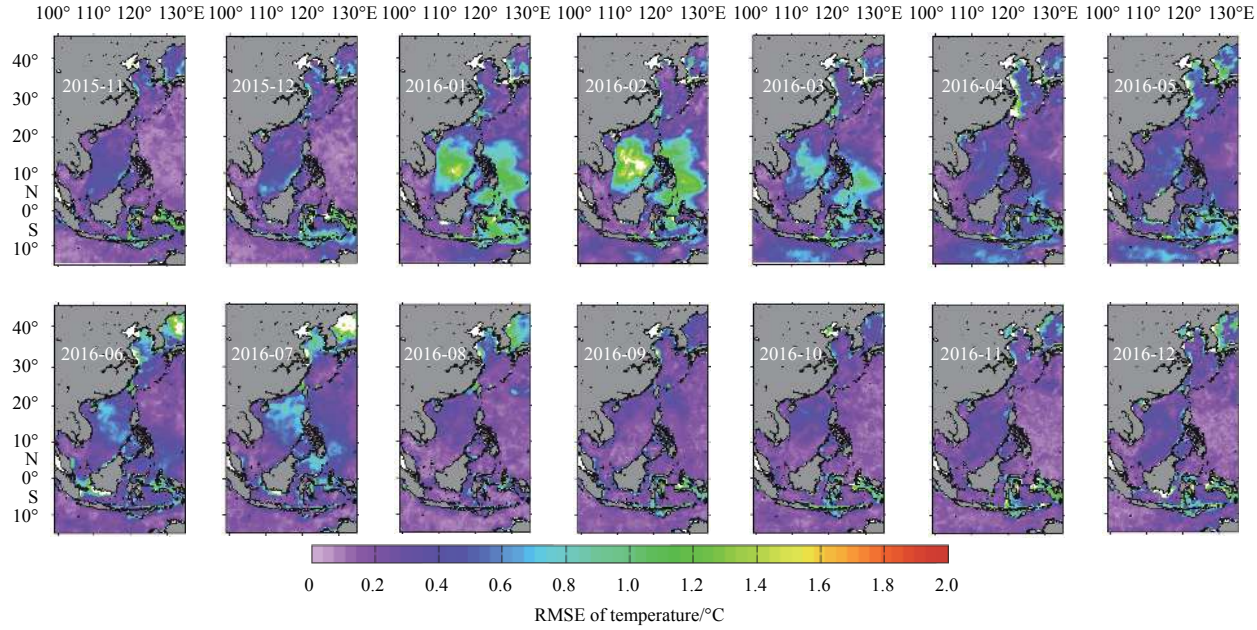

Fig. 11. Spatial distribution of RMSE between the monthly mean OISST and the monthly mean 72-h forecasting results.

Table 5. Statistical analysis of the coherence for temperature between observation and 72-h forecasting results

Data	Temperature		
	MAE/°C	RE/%	RMSE/°C
OISST	0.49	2.12	0.62
Argo	0.19	2.74	0.61

(12.54°), for the bottom layer (36 m) is 0.04 m/s (7.21°).

4 Conclusions

Based on the COAWST modeling system and the MASNUM wave model, a 72-h fine-resolution coupled atmosphere-wave-ocean forecasting system was developed for the South China Sea and its adjacent seas. Several improvements are made. The wave-induced mixing B_v and the internal wave induced vertical mixing are considered by adding to the KPP mixing scheme directly for the ROMS model to improve simulation of the structure of temperature and salinity. To get precise initial conditions for the wave and current model in the coupled forecasting system, a stand-alone MASNUM wave model and a stand-alone ROMS model are set up, respectively. The EAKF data assimilation method was adopted for the MASNUM wave model with assimilating Jason-2 SWH data. For the ocean model, firstly, the climatological simulation is integrated 40 years for spin-up. Secondly, the hindcast simulation initialized from the end month of climato-

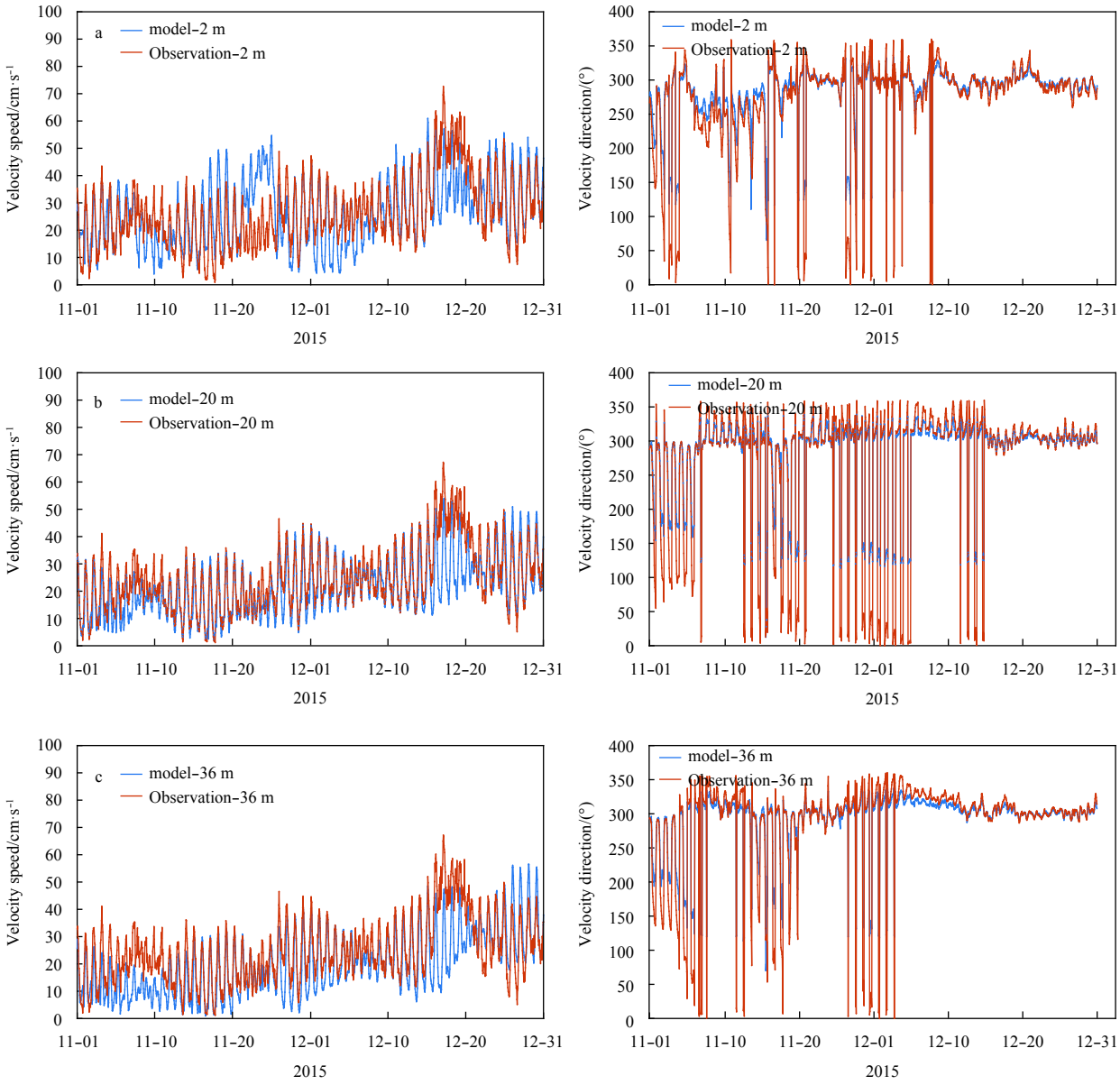

Fig. 12. Comparison of velocity speed and direction between observation (red line) and 72-h forecasting results (blue line). The observing station is located in the Karimata Strait. a. 2 m, b. 20 m and c. 36 m.

Table 6. Statistical analysis of the coherence for velocity speed and direction between observation and 72-h forecasting results

Depth/m	Velocity speed			Velocity direction		
	MAE/ m·s^{-1}	RE/ %	RMSE/ m·s^{-1}	MAE/ (°)	RE/ %	RMSE/ (°)
2	0.13	21.82	0.21	12.54	4.22	17.21
20	0.09	20.65	0.19	1.69	0.56	6.00
36	0.04	19.80	0.07	7.21	2.41	10.14
Average	0.09	20.76	0.16	7.15	2.40	11.12

logy run and were integrated from January 2014 to October 2015. The EAKF data assimilation method was also introduced to the ROMS model with using a random field scheme to construct the wind forcing field ensemble. Then the pre-24-h assimilated ocean hindcast simulation was run to provide the initial condition for the coupled forecasting system. After the initial fields for the SWAN model and ROMS model have been generated, the 72-h coupled forecasting model was run operationally. Reasonable agreement of simulation results with field observation results verified the reliability of the model. The forecasting products can provide service for the shipping safety, the fisheries and the oil exploitation.

References

Aldrian E, Sein D, Jacob D, et al. 2005. Modelling Indonesian rainfall with a coupled regional model. Climate Dynamics, 25(1): 1–17, doi: 10.1007/s00382-004-0483-0

Anderson J L. 2001. An ensemble adjustment Kalman filter for data assimilation. Monthly Weather Review, 129(12): 2884–2903, doi: 10.1175/1520-0493(2001)129<2884:AEAKFF>2.0.CO;2

Anderson J L. 2003. A local least squares framework for ensemble filtering. Monthly Weather Review, 131(4): 634–642, doi: 10.1175/1520-0493(2003)131<0634:ALLSFF>2.0.CO;2

Booij N, Ris R C, Holthuijsen L H. 1999. A third-generation wave

model for coastal regions: 1. Model description and validation. Journal of Geophysical Research: Oceans, 104(C4): 7649–7666, doi: 10.1029/98JC02622

Boville B A, Gent P R. 1998. The NCAR climate system model, version one. Journal of Climate, 11(6): 1115–1130, doi: 10.1175/1520-0442(1998)011<1115:TNCSMV>2.0.CO;2

Bruneau N, Toumi R. 2016. A fully-coupled atmosphere-ocean-wave model of the Caspian Sea. Ocean Modelling, 107: 97–111, doi: 10.1016/j.ocemod.2016.10.006

Bryan K, Manabe S, Pacanowski R C. 1975. A global ocean-atmosphere climate model. Part II. The oceanic circulation. Journal of Physical Oceanography, 5(1): 30–46, doi: 10.1175/1520-0485(1975)005<0030:AGOACM>2.0.CO;2

Carnes M R. 2009. Description and Evaluation of GDEM-V 3.0. NRL Rep, 2009: NRL/MR/7330-09-9165. Washington DC: Naval Research Lab Stennis Space Center

Chassignet E P, Arango H, Dietrich D, et al. 2003. DAMEE-NAB: the base experiments. Dynamics of Atmospheres and Oceans, 32(3–4): 155–183

Chen F, Dudhia J. 2001. Coupling an advanced land surface–hydrology model with the Penn State–NCAR MM5 modeling system: Part II. Preliminary model validation. Monthly Weather Review, 129(4): 587–604, doi: 10.1175/1520-0493(2001)129<0587:CAALSH>2.0.CO;2

Collins W D, Bitz C M, Blackmon M L, et al. 2006. The community climate system model version 3 (CCSM3). Journal of Climate, 19(11): 2122–2143, doi: 10.1175/JCLI3761.1

Diaz H F, Folland C K, Manabe T, et al. 2002. Workshop on advances in the use of historical marine climate data . World Meteorological Organization Bulletin, 51: 377–380

Döscher R, Willén U, Jones C, et al. 2002. The development of the regional coupled ocean-atmosphere model RCAO. Boreal Environment Research, 7(3): 183–192

Dudhia J. 2004. The weather research and forecasting model (version 2.0). In: Proceedings of the 2nd International Workshop on Next Generation NWP Model. Seoul: Yonsei University, 19–23

Evensen G. 1994. Sequential data assimilation with a nonlinear quasi-geostrophic model using Monte Carlo methods to forecast error statistics. Journal of Geophysical Research, 99(5): 10143–10162

Evensen G. 2003. The ensemble Kalman filter: Theoretical formulation and practical implementation. Ocean Dynamics, 53(4): 343–367, doi: 10.1007/s10236-003-0036-9

Gustafsson N, Nyberg L, Omstedt A. 1998. Coupling of a high-resolution atmospheric model and an ocean model for the Baltic Sea. Monthly Weather Review, 126(11): 2822–2846, doi: 10.1175/1520-0493(1998)126<2822:COAHRA>2.0.CO;2

Hagedorn R, Lehmann A, Jacob D. 2000. A coupled high resolution atmosphere-ocean model for the BALTEX region. Meteorologische Zeitschrift, 9(1): 7–20, doi: 10.1127/metz/9/2000/7

Haidvogel D B, Arango H, Budgell W P, et al. 2008. Ocean forecasting in terrain-following coordinates: Formulation and skill assessment of the Regional Ocean Modeling System. Journal of Computational Physics, 227(7): 3595–3624, doi: 10.1016/j.jcp.2007.06.016

Haidvogel D B, Arango H G, Hedstrom K, et al. 2002. Model evaluation experiments in the North Atlantic Basin: simulations in nonlinear terrain-following coordinates. Dynamics of Atmospheres and Oceans, 32(3–4): 239–281

Hasselmann K, Barnett T P, Bouws E, et al. 1973. Measurements of wind-wave growth and swell decay during the Joint North Sea Wave Project (JONSWAP). Deutsche Hydrographische Zeitschrift, A8(12): 1–95

Hodur R M. 1997. The Naval Research Laboratory's coupled ocean/atmosphere mesoscale prediction system (COAMPS). Monthly Weather Review, 125(7): 1414–1430, doi: 10.1175/1520-0493(1997)125<1414:TNRLSC>2.0.CO;2

Hong Songyou, Pan Hualu. 1998. Convective trigger function for a mass-flux cumulus parameterization scheme. Monthly Weather Review, 126(10): 2599–2620, doi: 10.1175/1520-0493(1998)126<2599:CTFFAM>2.0.CO;2

Hong S Y, Kim J H, Lim J O, et al. 2006. The WRF single moment microphysics scheme (WSM). Journal of the Korean Meteorological Society, 42: 129–151

Janjic Z I. 1996. The surface layer in the NCEP Eta model. In: Eleventh Conference on Numerical Weather Prediction. Norfolk: American Meteorological Society, 19–23

Janjic Z I. 2002. Nonsingular implementation of the Mellor-Yamada level 2. 5 scheme in the NCEP Meso-scale model. NCEP Office Note, 437: 61

Kain J S. 2004. The Kain Fritsch convective parameterization: an update. Journal of Applied Meteorology, 43(1): 170–181, doi: 10.1175/1520-0450(2004)043<0170:TKCPAU>2.0.CO;2

Laurent L. 2008. Turbulent dissipation on the margins of the South China Sea. Geophysical Research Letters, 35(23): L23615, doi: 10.1029/2008GL035520

Manabe S, Bryan K. 1969. Climate calculations with a combined ocean-atmosphere model. Journal of the Atmospheric Sciences, 26(4): 786–789, doi: 10.1175/1520-0469(1969)026<0786:CCWACO>2.0.CO;2

Manabe S, Bryan K, Spelman M J. 1975. A global ocean-atmosphere climate model. Part I. The atmospheric circulation. Journal of Physical Oceanography, 5(1): 3–29, doi: 10.1175/1520-0485(1975)005<0003:AGOACM>2.0.CO;2

Mlawer E J, Taubman S J, Brown P D, et al. 1997. Radiative transfer for inhomogeneous atmospheres: RRTM, a validated correlated-k model for the longwave. Journal of Geophysical Research: Atmospheres, 102(D14): 16663–16682, doi: 10.1029/97JD00237

Neelin J D, Latif M, Allaart M A F, et al. 1992. Tropical air-sea interaction in general circulation models. Climate Dynamics, 7(2): 73–104, doi: 10.1007/BF00209610

Qiao Fangli, Yuan Yeli, Ezer T, et al. 2010. A three-dimensional surface wave–ocean circulation coupled model and its initial testing. Ocean Dynamics, 60(5): 1339–1355, doi: 10.1007/s10236-010-0326-y

Qiao Fangli, Yuan Yeli, Yang Yongzeng, et al. 2004. Wave-induced mixing in the upper ocean: Distribution and application to a global ocean circulation model. Geophysical Research Letters, 31(11): L11303

Sasaki H, Kurihara K, Takayabu I, et al. 2006. Preliminary results from the coupled atmosphere-ocean regional climate model at the meteorological research institute. Journal of the Meteorological Society of Japan, 84(2): 389–403, doi: 10.2151/jmsj.84.389

Shchepetkin A F, McWilliams J C. 2005. The regional oceanic modeling system (ROMS): a split-explicit, free-surface, topography-following-coordinate oceanic model. Ocean Modelling, 9(4): 347–404, doi: 10.1016/j.ocemod.2004.08.002

Shchepetkin A F, McWilliams J C. 2009. Correction and commentary for "Ocean forecasting in terrain-following coordinates: Formulation and skill assessment of the regional ocean modeling system" by Haidvogel et al., J. Comp. Phys. 227, pp. 3595–3624. Journal of Computational Physics, 228(24): 8985–9000, doi: 10.1016/j.jcp.2009.09.002

Schrum C, Hübner U, Jacob D, et al. 2003. A coupled atmosphere/ice/ocean model for the North Sea and the Baltic Sea. Climate Dynamics, 21(2): 131–151, doi: 10.1007/s00382-003-0322-8

Seo H, Miller A J, Roads J O. 2007. The Scripps Coupled Ocean–Atmosphere Regional (SCOAR) model, with applications in the eastern Pacific sector. Journal of Climate, 20(3): 381–402, doi: 10.1175/JCLI4016.1

Skamarock W C, Klemp J B, Dudhia J, et al. 2005. A Description of the Advanced Research WRF Version 2. Available from NCAR; P O BOX 3000. Boulder, CO, Vol 88, 7–25

Sun Meng, Yin Xunqiang, Yang Yongzeng. 2014. Construction and application in global wave data assimilation of static sample set. Oceanologia et Limnologia Sinica (in Chinese), 45(5): 918–927

Sun Meng, Yin Xunqiang, Yang Yongzeng, et al. 2017. An effective method based on dynamic sampling for data assimilation in a global wave model. Ocean Dynamics, 67(3–4): 433–449

Wang Guansuo, Qiao Fangli, Xia Changshui. 2010a. Parallelization of a coupled wave-circulation model and its application. Ocean

Dynamics, 60(2): 331–339, doi: 10.1007/s10236-010-0274-6

Wang Yonggang, Qiao Fangli, Fang Guohong, et al. 2010b. Application of wave-induced vertical mixing to the K profile parameterization scheme. Journal of Geophysical Research: Oceans, 115(C9): C09014

Warner J C, Armstrong B, He Ruoying, et al. 2010. Development of a coupled ocean–atmosphere–wave–sediment transport (COAWST) modeling system. Ocean Modelling, 35(3): 230–244, doi: 10.1016/j.ocemod.2010.07.010

Warner J C, Sherwood C R, Signell R P, et al. 2008. Development of a three-dimensional, regional, coupled wave, current, and sediment-transport model. Computers & Geosciences, 34(10): 1284–1306

Washington W M, Semtner A J Jr, Meehl G A, et al. 2010. A general circulation experiment with a coupled atmosphere, ocean and sea ice model. Journal of Physical Oceanography, 10(12): 1887–1908

Yang Yongzeng, Qiao Fangli, Zhao Wei, et al. 2005. MASNUM ocean wave numerical model in spherical coordinates and its application. Haiyang Xuebao (in Chinese), 27(2): 1–7

Yang Qingxuan, Zhao Wei, Liang Xinfeng, et al. 2016. Three-dimensional distribution of turbulent mixing in the South China Sea. Journal of Physical Oceanography, 46(3): 769–788, doi: 10.1175/JPO-D-14-0220.1

Yin Xunqiang, Qiao Fangli, Yang Yongzeng, et al. 2010. An ensemble adjustment Kalman filter study for Argo data. Chinese Journal of Oceanology and Limnology, 28(3): 626–635, doi: 10.1007/s00343-010-9017-2

Yuan Yeli, Hua Feng, Pan Zengdi, et al. 1992. LAGFD-WAM numerical wave model-II. Characteristics inlaid scheme and its application. Acta Oceanologica Sinica, 11(1): 13–23

Yuan Yeli, Pan Zengdi, Hua Feng, et al. 1991. LAGFD-WAM numerical wave model-I. basic physical model. Acta Oceanologica Sinica, 10(4): 483–488

Yuan Yeli, Tung C C, Huang N E. 1986. Statistical characteristics of breaking waves. In: Phillips O M, Hasselmann K, eds. Wave Dynamics and Radio Probing of the Ocean Surface. Boston, MA: Springer, 265–272

Appendix:

Statistical analysis methods are applied to compare forecast product (P_i) with observations (O_i) quantitatively.

Mean absolute error (MAE) is defined by

$$\mathrm{MAE} = \frac{1}{N}\sum_{i=1}^{N}|P_i - O_i|\,.$$

Relative error (RE) is defined by

$$\mathrm{RE} = \frac{\frac{1}{N}\sum_{i=1}^{N}(P_i - O_i)}{\bar{O}}\,.$$

Root-mean-square error (RMSE) is defined by

$$\mathrm{RMSE} = \sqrt{\frac{1}{N}\sum_{i=1}^{N}(P_i - O_i)^2}.$$